

## Electron acceleration using intense electromagnetic waves

C. R. Menyuk, A. T. Drobot, K. Papadopoulos, and H. Karimabadi

Citation: *Physics of Fluids (1958-1988)* **31**, 3768 (1988); doi: 10.1063/1.866896

View online: <http://dx.doi.org/10.1063/1.866896>

View Table of Contents: <http://scitation.aip.org/content/aip/journal/pof1/31/12?ver=pdfcov>

Published by the [AIP Publishing](#)

---

### Articles you may be interested in

[Relativistic electron beam acceleration by nonlinear scattering of electromagnetic waves in a magnetized plasma](#)

*Phys. Plasmas* **15**, 013104 (2008); 10.1063/1.2825000

[Electron acceleration by transverse electromagnetic wave supplemented with crossed static magnetic field](#)

*AIP Conf. Proc.* **369**, 678 (1996); 10.1063/1.50544

[Relativistic electron beam acceleration by nonlinear Landau damping of electromagnetic waves](#)

*AIP Conf. Proc.* **369**, 1216 (1996); 10.1063/1.50406

[Electron beam acceleration by nonlinear Landau damping of electromagnetic waves in a plasma](#)

*Phys. Fluids B* **5**, 201 (1993); 10.1063/1.860972

[Electron acceleration by electromagnetic waves in a weakly magnetized inhomogeneous plasma](#)

*Phys. Fluids* **28**, 1574 (1985); 10.1063/1.864945

---



**HAVE YOU HEARD?**

Employers hiring scientists  
and engineers trust  
**physicstodayJOBS**



<http://careers.physicstoday.org/post.cfm>

# Electron acceleration using intense electromagnetic waves

C. R. Menyuk,<sup>a)</sup> A. T. Drobot, and K. Papadopoulos<sup>b)</sup>

*Science Applications International Corporation, 1710 Goodridge Drive, McLean, Virginia 22102*

H. Karimabadi

*Institute of Geophysics and Planetary Physics, University of California, Los Angeles, California 90024*

(Received 12 August 1987; accepted 18 August 1988)

Electron acceleration by an intense electromagnetic wave incident obliquely to the ambient magnetic field in a plasma is considered. It is shown that the wave amplitude has a stochasticity inducing threshold. Although substantial acceleration can be achieved below this threshold, it is limited to the trapping width of a single resonance. Above threshold, the electrons can accelerate from resonance to resonance. It is also shown that when the parallel phase velocity of the electromagnetic waves is supraluminous, the Hamiltonian surfaces describing the wave-particle interaction are topologically open. In this case, electrons gain large amounts of energy. The mechanism is quite robust, being weakly sensitive to changes in the wave parameters and the electron's initial energy; as a result, it is an ideal mechanism for space applications. As an application, the conditions are obtained for accelerating electrons to energies of several MeV using ground-based transmitters.

## I. INTRODUCTION

Few phenomena span a wider range of laboratory and astrophysical applications than charged particle acceleration. Prominent among the acceleration processes is plasma acceleration due to electromagnetic waves. The presence of a magnetic field allows for resonance to be accomplished via the cyclotron motion and thus provides the means for direct particle acceleration by electromagnetic waves. Indeed, early studies<sup>1,2</sup> indicated that "unlimited" coherent electron acceleration can be accomplished by an electromagnetic wave of frequency  $\omega$  and wavenumber  $k$  if (1) the electromagnetic wave propagates parallel to the magnetic field; (2) the index of refraction  $n = kc/\omega \approx 1$ ; and (3) the electron velocity  $v$  initially satisfies the resonance condition,

$$\omega - \omega_c/\gamma - kv_z = 0. \quad (1)$$

To obtain Eq. (1), we have assumed an ambient magnetic field  $\mathbf{B} = B_0\hat{e}_z$ , denoted the nonrelativistic gyrofrequency by  $\omega_c = eB_0/mc$ , and denoted the relativistic factor by

$$\gamma = (1 - v^2/c^2)^{-1/2}, \quad (2)$$

where  $e$  and  $m$  are the electron charge and mass, respectively. Coherent acceleration has been thought to play a role in astrophysical<sup>3,4</sup> as well as in laboratory<sup>5</sup> plasmas.

Unfortunately, even slight violations of the three conditions just described lead to a sharp deterioration of the obtainable electron energies. Hence this mechanism requires delicate control of the plasma parameters, the wave characteristics, and the electron injection energies. Such control can be achieved in the laboratory, but is not possible in space when considering either naturally occurring<sup>3</sup> or artificially created<sup>6</sup> electromagnetic waves. In particular, one has no control over the initial electron energies, and satisfying Eq.

(1) even approximately appears difficult, if not impossible. We should mention that similar difficulties arise in applying new concepts of plasma accelerators, such as the beat wave acceleration<sup>7</sup> and surfatron<sup>8</sup> which, while well suited to the laboratory, do not appear well suited to most space applications.

It is the purpose of this paper to discuss a novel stochastic electron acceleration mechanism resulting from the interaction of plasma electrons with an electromagnetic wave propagating obliquely to an ambient magnetic field. It is shown that, in this case, the electron motion is stochastic. When, in addition, the parallel phase velocity of the wave is supraluminous, i.e.,  $k_{\parallel}c/\omega < 1$ , the Hamiltonian surfaces are topologically open, and it is possible to accelerate electrons to large energies. The supraluminous case contrasts sharply with the well-studied subluminal case<sup>9,10</sup> where the Hamiltonian surfaces are topologically closed and the maximum energy gain is severely limited. This stochastic mechanism is quite robust; electrons gain large energies over a wide range in plasma parameters, wave characteristics (including a spread in frequency), and initial particle energies—including zero initial kinetic energy. However, the energy gain is diffusive and thus occurs over longer length and time scales than coherent acceleration. As a consequence, the stochastic mechanism appears less well suited than coherent mechanisms to laboratory applications where length and time scales must be minimized.

The properties of the acceleration process, including the threshold wave amplitude for stochastic electron acceleration and the maximum obtainable electron energy, are determined by Hamiltonian techniques. We introduce "resonance diagrams," a graphical technique based on the well-known resonance overlap criterion.<sup>11</sup> This technique allows us to avoid solving the electron's equations of motion, which results in enormous savings in computer time, and, as a result, makes it possible for us to explore a wide parameter range. It also allows us to gain insight into the global proper-

<sup>a)</sup> Permanent address: Department of Electrical Engineering, University of Maryland, Baltimore, Maryland 21228.

<sup>b)</sup> Permanent address: Department of Physics and Astronomy, University of Maryland, College Park, Maryland 20741.

ties of the phase space that would be difficult to obtain from direct study of particle orbits. This technique is, however, perturbative and requires validation by direct comparison with single particle orbits. The accuracy of the resonance diagram technique was tested successfully by comparing the results for selected cases against surface-of-section plots<sup>12</sup> produced from single particle orbits.

In this paper we extend the results of previous work<sup>6</sup> by determining, in substantially more detail, the variation of the stochasticity threshold and the maximum attainable energy as the wave propagation angle, the wave intensity, the wave frequency, the ambient magnetic field strength, and the plasma frequency all vary. It is shown that while large amounts of energy can be gained below the stochasticity threshold when electrons are resonant with cyclotron harmonics, this energy gain is restricted to a single resonant trapping width. Above threshold, electrons can move freely from resonance to resonance leading to much higher energy gains over a sufficiently long length and time scale. We also correct errors that appeared in our previous work.<sup>6</sup>

As an application of these results, we consider the remote acceleration of ionospheric electrons from ground-based radio transmitters. Accelerated electrons could be used to create an artificial aurora, to probe the magnetosphere, and to measure the cross sections of ionospheric constituents interacting with energetic electrons. Such experiments have been carried out to date from rocket and shuttle borne accelerators<sup>13,14</sup> and have a number of drawbacks. As part of this application we have carried out a statistical study of single particle orbits in order to determine the length and time scales necessary to achieve a high flux of multi-mega-electron-volt electrons.

The remainder of this paper is organized as follows. In Sec. II we introduce the Hamiltonian formalism and determine the resonance locations in phase space and the conditions for their overlap. In Sec. III we determine the maximum obtainable electron energies over a wide range of parameters using resonance diagrams and surface-of-section plots. In Sec. IV we apply our results to the ionosphere and determine the time and length scales necessary to obtain substantial acceleration. We present our conclusions in Sec. V.

## II. HAMILTONIAN FORMULATION

The Hamiltonian governing electron motion in the field of an electromagnetic wave may be written

$$H = mc^2\gamma = mc^2[(\mathbf{p}/mc + e\mathbf{A}/mc^2)^2 + 1]^{1/2}, \quad (3)$$

where, letting

$$\psi = k_{\perp}x + k_{\parallel}z - \omega t \quad (4)$$

represent the phase of the wave front, we find

$$\mathbf{A} = A[(k_{\parallel}/k)\sin\psi\hat{\mathbf{e}}_x + \cos\psi\hat{\mathbf{e}}_y - (k_{\perp}/k)\sin\psi\hat{\mathbf{e}}_z] + xB_0\hat{\mathbf{e}}_z. \quad (5)$$

The ambient magnetic field  $B_0$  is taken in the  $z$  direction, and  $\mathbf{p}$  is the *canonical* momentum. The perpendicular and parallel wavenumbers are defined by  $k_{\perp} = k \sin \alpha$  and  $k_{\parallel} = k \cos \alpha$ , respectively, where  $\alpha$  is the angle of propagation. We have assumed, in obtaining Eq. (5), that the wave is

right circularly polarized, which is optimum for coupling to electrons. We further assume that  $\omega$  and  $k$  are related through the dispersion relation

$$kc/\omega = [1 - \omega_p^2/\omega(\omega - \omega_c)]^{1/2}, \quad (6)$$

where  $\omega_p$  is the plasma frequency. This dispersion relation is strictly valid only for circularly polarized waves. Elsewhere<sup>15</sup> we have considered the consequences of including the full electromagnetic wave variation and shown that it leads to little change in the cases considered here. Full details will be published elsewhere.

To further analyze the Hamiltonian, we make a canonical transformation eliminating the explicit time dependence. The generating function is<sup>16</sup>

$$F = p'_z[z - (\omega/k_{\parallel})t], \quad (7)$$

leading to the new variables and Hamiltonian

$$z' = z - (\omega/k_{\parallel})t, \quad p'_z = p_z, \quad H' = H - (\omega/k_{\parallel})p_z. \quad (8)$$

Dropping the primes, the Hamiltonian has the form

$$H = mc^2\gamma - (\omega/k_{\parallel})p_z. \quad (9)$$

The electromagnetic field has the same form as in Eq. (5), but the phase  $\psi$  becomes

$$\psi = k_{\perp}x + k_{\parallel}z. \quad (10)$$

Physically this transformation is equivalent to making a Lorentz transformation into the frame where the  $z$  dependence is eliminated and then transforming so that the proper time is replaced by  $z$ .

The quantities  $H$  and  $p_y$  are constants of the motion. We now eliminate  $p_y$  by absorbing it into  $x$ , reducing the problem to two degrees of freedom. Explicitly,

$$\gamma = \left[ 1 + \left( \frac{p_x}{mc} + \frac{ek_{\parallel}A}{kmc^2} \sin \psi \right)^2 + \left( \frac{p_y}{mc} + \frac{eA}{mc^2} \cos \psi + x \frac{eB_0}{mc^2} \right)^2 + \left( \frac{p_z}{mc} - \frac{ek_{\perp}A}{kmc^2} \sin \psi \right)^2 \right]^{1/2}. \quad (11)$$

Defining the generating function

$$F = p'_x \left( x + \frac{cp'_y}{eB_0} \right) + yp'_y + p'_z \left( z - \frac{k_{\perp}}{k_{\parallel}} \frac{cp'_y}{eB_0} \right), \quad (12)$$

we find

$$\begin{aligned} x' &= x + \frac{cp'_y}{eB_0}, & p'_x &= p_x, \\ y' &= y + \frac{cp'_x}{eB_0} - \frac{k_{\perp}}{k_{\parallel}} \frac{cp'_z}{eB_0}, & p'_y &= p_y, \\ z' &= z - \frac{k_{\perp}}{k_{\parallel}} \frac{cp'_y}{eB_0}, & p'_z &= p_z. \end{aligned} \quad (13)$$

Note that, unlike  $y$ ,  $y'$  is a constant of the motion. Dropping the primes,  $\gamma$  becomes

$$\gamma = \left[ 1 + \left( \frac{p_x}{mc} + \frac{ek_{\parallel}A}{kmc^2} \sin \psi \right)^2 + \left( \frac{eA}{mc^2} \cos \psi + x \frac{eB_0}{mc^2} \right)^2 + \left( \frac{p_z}{mc} - \frac{ek_{\perp}A}{kmc^2} \sin \psi \right)^2 \right]^{1/2}. \quad (14)$$

The quantity  $\psi$  still has the form given by Eq. (10).

Since  $\gamma$  is quadratic in both  $x$  and  $p_x$ , it is appropriate to make a transformation to action-angle variables  $(p_x, x) \rightarrow (J, \theta)$ , where

$$\begin{aligned} p_x &= (2eB_0 J/c)^{1/2} \cos \theta, \\ x &= (2cJ/eB_0)^{1/2} \sin \theta. \end{aligned} \quad (15)$$

This transformation is canonical. It will be useful hereafter to define the auxiliary quantities

$$p_{\perp} = (2eB_0 J/c)^{1/2}, \quad p_{\parallel} = p_z, \quad \rho = (2cJ/eB_0)^{1/2}. \quad (16)$$

Using these new variables, Eq. (14) becomes

$$\gamma = \left[ 1 + \frac{p_{\perp}^2}{m^2 c^2} + \frac{p_{\parallel}^2}{m^2 c^2} + 2 \frac{eA}{mc^2} \left( \frac{p_{\perp}}{mc} \cos \theta \sin \psi \cos \alpha + \frac{p_{\parallel}}{mc} \sin \theta \cos \psi - \frac{p_{\parallel}}{mc} \sin \psi \sin \alpha \right) + \left( \frac{eA}{mc^2} \right)^2 \right]^{1/2}, \quad (17)$$

where

$$\psi = k_{\parallel} z + k_{\perp} \rho \sin \theta. \quad (18)$$

We now expand Eq. (17) as a power series in  $\epsilon = eA/mc^2$ . At zeroth order,

$$H = H_0 = mc^2 \gamma_0 - (\omega/k_{\parallel}) p_{\parallel}, \quad (19)$$

where

$$\gamma_0 = (1 + p_{\perp}^2/m^2 c^2 + p_{\parallel}^2/m^2 c^2)^{1/2}. \quad (20)$$

At first order, we first define

$$\begin{aligned} \alpha_l &= (mc^2/\gamma_0) \{ (\omega_c \rho/2c) [J_{l-1}(k_{\perp} \rho)(1 + \cos \alpha) - J_{l+1}(k_{\perp} \rho)(1 - \cos \alpha)] \\ &\quad - (p_{\parallel}/mc) \sin \alpha J_l(k_{\perp} \rho) \}, \end{aligned} \quad (21)$$

where  $J_l(x)$  is the  $l$ th Bessel function of the first kind. We now obtain

$$H = H_0 + \epsilon H_1, \quad (22)$$

where

$$H_1 = \sum_{l=-\infty}^{\infty} a_l \sin(k_{\parallel} z + l\theta). \quad (23)$$

From Eqs. (19) and (20), it follows that the zeroth-order Hamiltonian surfaces are hyperbolas in  $p_{\parallel}$ - $p_{\perp}$  space when  $n_{\parallel} = k_{\parallel} c/\omega < 1$  and are ellipses when  $n_{\parallel} = k_{\parallel} c/\omega > 1$ .

We consider next the resonance surfaces. These occur when

$$[k_{\parallel} \dot{z} + l\dot{\theta}]|_0 = 0, \quad (24)$$

where

$$\dot{z}|_0 = \frac{\partial H_0}{\partial p_z} \quad \text{and} \quad \dot{\theta}|_0 = \frac{\partial H_0}{\partial J}, \quad (25)$$

or, in other words, when

$$\frac{\omega}{\omega_c} \gamma_0 - \frac{k_{\parallel}}{\omega_c} \frac{p_{\parallel}}{m} = l. \quad (26)$$

Comparing Eq. (19) with Eq. (26), one readily verifies that the resonance surfaces are elliptic when the zeroth-order Hamiltonian surfaces are hyperbolic and vice versa. When both are parabolic, they lie on top of each other.

We compute next the resonance widths using the standard approach described by Chirikov.<sup>11</sup> Assuming first that the resonances are well separated so that a single resonance can be considered in isolation, we obtain

$$H = H_0 + \epsilon a_l \sin(k_{\parallel} z + l\theta). \quad (27)$$

We next perform a canonical transformation that eliminates  $\theta$  from the Hamiltonian. The generating function

$$F = p'_z [z + (l/k_{\parallel})\theta] + J'\theta \quad (28)$$

yields the new canonical variables

$$\begin{aligned} z' &= z + (l/k_{\parallel})\theta, \quad p'_z = p_z, \\ \theta' &= \theta, \quad J' = J - (l/k_{\parallel})p_z. \end{aligned} \quad (29)$$

The quantity  $J'$  is a constant of the motion. We now focus on a specific point  $(p_{\parallel,0}, p_{\perp,0})$  lying on the  $l$ th resonance surface. Expanding  $H_0$  in a Taylor expansion in  $p_z$  about that point, we obtain

$$\begin{aligned} H_0 &= H_0^0 + \left. \frac{\partial H_0}{\partial p_z} \right|_{J'} (p_z - p_{z,0}) \\ &\quad + \frac{1}{2} \left. \frac{\partial^2 H_0}{\partial p_z^2} \right|_{J'} (p_z - p_{z,0})^2. \end{aligned} \quad (30)$$

Noting that

$$\left. \frac{\partial H_0}{\partial p_z} \right|_{J'} = 0, \quad (31)$$

and

$$\left. \frac{\partial^2 H_0}{\partial p_z^2} \right|_{J'} \equiv \frac{1}{M} = \frac{1}{m\gamma_0} \left( 1 - \frac{\omega^2}{k_{\parallel}^2 c^2} \right), \quad (32)$$

we finally conclude

$$H = H_0^0 + (1/2M)(p_z - p_{z,0})^2 + \epsilon a_l \sin(k_{\parallel} z). \quad (33)$$

It immediately follows that

$$w = 4|\epsilon M a_l|^{1/2}, \quad (34)$$

where  $w$  is the width of the  $l$ th resonance. While use of this width leads to an overestimate of the point at which stochastic particle motion from resonance to resonance first becomes possible,<sup>11</sup> a comparison with surface-of-section plots of single particle orbits shows that it does provide a good estimate of when a *significant* number of particles in the neighborhood of the resonance are free to move stochastically from resonance to resonance. It is interesting to note that  $w$  becomes singular when both the Hamiltonian and resonance surfaces are parabolic; i.e.,  $n_{\parallel} = k_{\parallel} c/\omega = 1$ . This case can be dealt with by using an appropriate extension of our present methodology.<sup>15</sup> It will be discussed in detail elsewhere.

We have determined the location in  $p_{\parallel}$ - $p_{\perp}$  space of both the Hamiltonian and resonance surfaces, and computed the resonance widths. All the elements necessary to determine

when electron motion becomes stochastic are available. This task is carried out in the next section.

### III. RESONANCE DIAGRAMS AND SURFACE-OF-SECTION PLOTS

#### A. Resonance diagrams

From the analysis of the previous section, we conclude that the parameters that characterize the wave-particle interaction are given by the ratio of the quiver velocity to  $c$ ,  $\epsilon = eA/mc^2$ , the wave propagation angle with respect to the magnetic field  $\alpha$ , and the ratios of the plasma frequency and the wave frequency to the cyclotron frequency,  $\omega_p/\omega_c$  and  $\omega/\omega_c$ , respectively. The wavenumber  $k$  is then determined by the dispersion relation. In this study we concentrate on values of  $\omega$  for which  $\omega_p^2/[\omega(\omega - \omega_c)] < 1$  and  $\omega/\omega_c \geq 1.8$ ; in this range the dispersion relation [Eq. (6)] is a reasonable approximation. For  $\omega \approx \omega_c$ , the cyclotron resonance strongly influences the wave and dispersion relation, and Eq. (6) is no longer useful. For  $\omega < \omega_c$ , Eq. (6) can be used if  $\omega_p$  is very small, but the resonances are spaced too far apart to lead to resonance overlap.

Typical resonance diagrams that we use to represent graphically the theory of the previous section are shown in Figs. 1 and 2. The Hamiltonian surfaces given by Eq. (19) are shown as solid curves in the  $p_{\parallel} - p_{\perp}$  space, while the resonant surfaces given by Eq. (21) are shown by small dots. The large dots indicate the resonance widths and are the cornerstone of the resonance diagram technique. These widths al-

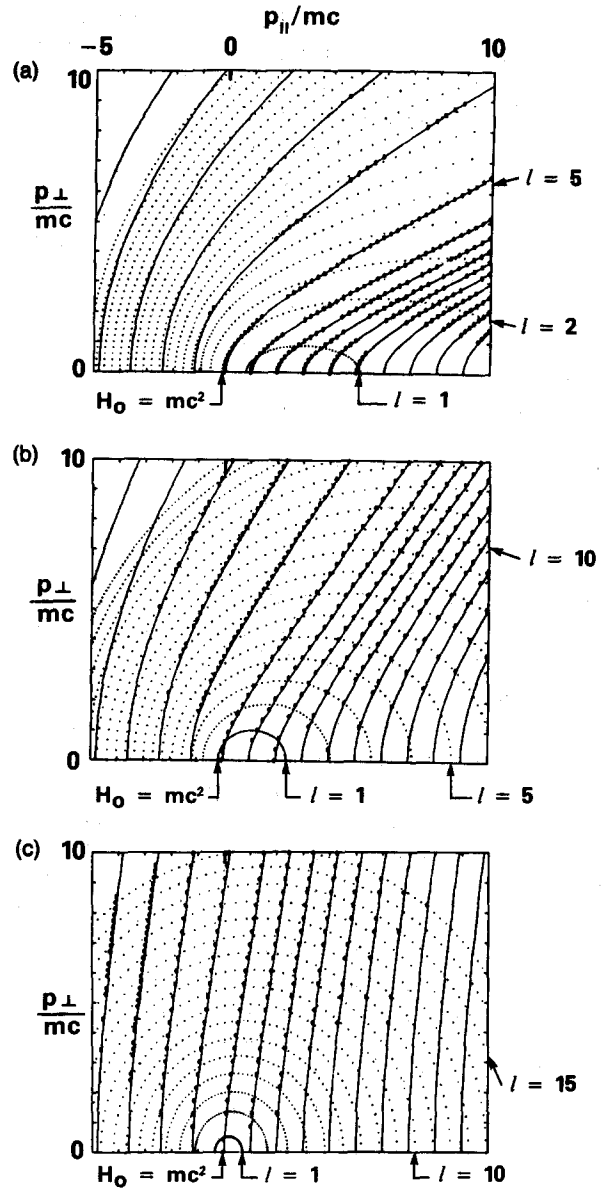


FIG. 2. Resonance diagrams ( $\omega/\omega_c = 1.8$ ,  $\omega_p/\omega_c = 0.3$ ,  $\epsilon = 0.1$ ). (a)  $\alpha = 20^\circ$ , (b)  $\alpha = 50^\circ$ , (c)  $\alpha = 80^\circ$ .

low one to determine by simple inspection the nature of the acceleration process and the maximum energy gain for a large array of different initial electron energies.

Resonance widths smaller than the spacing between large dots are not shown. When the large dots are continuously connected (i.e., are evenly spaced with no large gaps) in the neighborhood of only a single  $l$  resonance, the electron motion is regular. When they are continuously connected between several resonances, the electron motion is stochastic.

In Fig. 1, the parameters are  $\omega/\omega_c = 1.8$ ,  $\omega_p/\omega_c = 0.3$ , and  $\epsilon = 0.2$  at two different angles of propagation. The value  $\omega_p/\omega_c = 0.3$  corresponds roughly to the nighttime ionosphere at 130 km,<sup>17,18</sup> while  $\epsilon = 0.2$  corresponds to a power flux of 20 W/cm<sup>2</sup>. Paying particular attention to the  $H_0 = mc^2$  surface, on which electrons accelerated from zero initial kinetic energy are located, we see that when  $\alpha = 15^\circ$ , the resonances are separated, and an electron with zero ini-

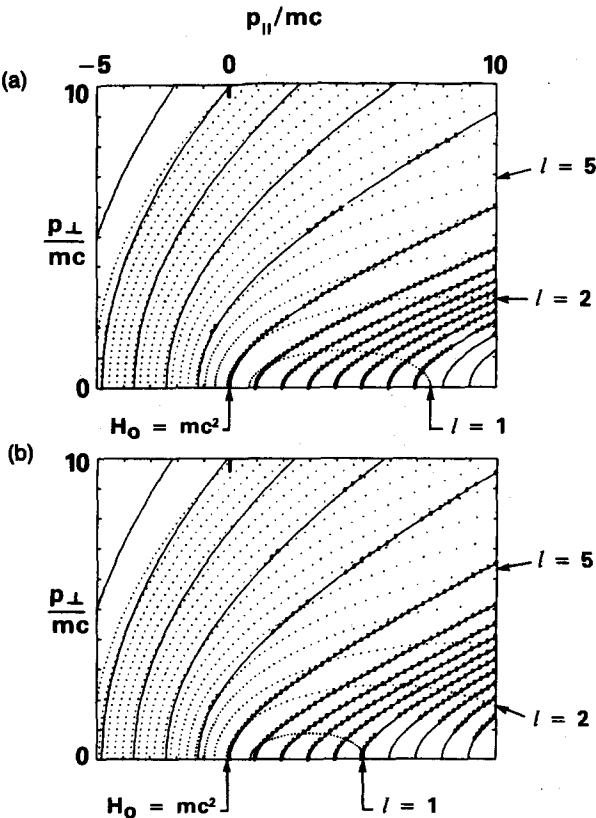


FIG. 1. Resonance diagrams ( $\omega/\omega_c = 1.8$ ,  $\omega_p/\omega_c = 0.3$ ,  $\epsilon = 0.2$ ). (a)  $\alpha = 15^\circ$ , (b)  $\alpha = 20^\circ$ .

tial kinetic energy is confined to the  $l = 2$  resonance. We note that even though the electron is confined, it gains substantial energy; in this case almost 1.5 MeV. When the angle  $\alpha = 20^\circ$ , all the resonances visible on the  $H_0 = mc^2$  surface overlap. At larger angles similar results are obtained. As a consequence, electrons with zero initial kinetic energy can gain substantially more than 5 MeV of energy.

The surfaces where  $H_0 \neq mc^2$  correspond to electrons with nonzero initial kinetic energy. From both Figs. 1(a) and 1(b) we observe that electrons which initially have a large, positive parallel momentum move stochastically and will accelerate to high energies, while electrons which initially have a large, negative parallel momentum do not gain energy.

Similar results are shown in Fig. 2 when  $\epsilon = 0.1$ , corresponding to a significantly lower power flux of  $5 \text{ W/cm}^2$ . Only the angles are increased. As  $\alpha$  increases from  $5^\circ$  to  $50^\circ$ , one finds that the resonances on the  $H_0 = mc^2$  surface all eventually overlap, indicating that at large angles, electrons with zero initial kinetic energy will gain 5 MeV or more. The resonance overlap persists up to  $80^\circ$  where a slight gap develops as shown in Fig. 2(c). As we will show in detail in Sec. IV, this gap does not mean that electrons cannot be accelerated up to 5 MeV. The gap is small, and a fraction of the electrons can accelerate "through the gap"; however, these electrons exhibit sticky behavior, so that their rate of energy gain is reduced. As we move off the  $H_0 = mc^2$  surface at large angles, we find from Figs. 2(b) and 2(c) that there is a cone of initial conditions where electrons can be accelerated to large energies. If  $p_{\parallel}$  is large, regardless of sign, and  $p_{\perp} = 0$  initially, then no significant acceleration occurs.

Examination of a large number of different cases indicates that acceleration on the  $H_0 = mc^2$  surface is almost always enhanced by using large angles of propagation. The only exceptions found are at angles greater than or approximately equal to  $80^\circ$ , where small gaps can develop at zero kinetic energy as shown in Fig. 2(c) when overlap at lower angles is weak. No such gap develops for the parameters of Fig. 1. This behavior contrasts sharply with the unlimited, coherent acceleration<sup>1,2</sup> that occurs when  $\alpha = 0^\circ$  and the index of refraction  $n = 1$ . From our point of view, unlimited acceleration occurs because the  $l = 1$  resonance surface—the only one that exists—coincides exactly with a Hamiltonian surface. An electron whose Hamiltonian has the right value will thus be swept away to infinity.

As the angle increases, the range of  $\Delta p$  where the electron is in the neighborhood of a single resonance decreases. At the same time, the separation between resonances decreases, so that it is easier for the electron to move from resonance to resonance. There is a trade-off between these two effects, and it is not evident *a priori* which effect will dominate; our results indicate that it is the latter in most cases.

We now consider the effect of varying  $\omega/\omega_c$  while fixing  $\omega_p/\omega_c = 0.3$ , corresponding to the strongly magnetized limit or the nighttime ionosphere at 130 km. In Fig. 3 we show resonance diagrams as  $\omega/\omega_c$  varies from 1.8 through 2.2 at  $\alpha = 20^\circ$ . These diagrams indicate that it is impossible to accelerate electrons to high energies from zero initial energy

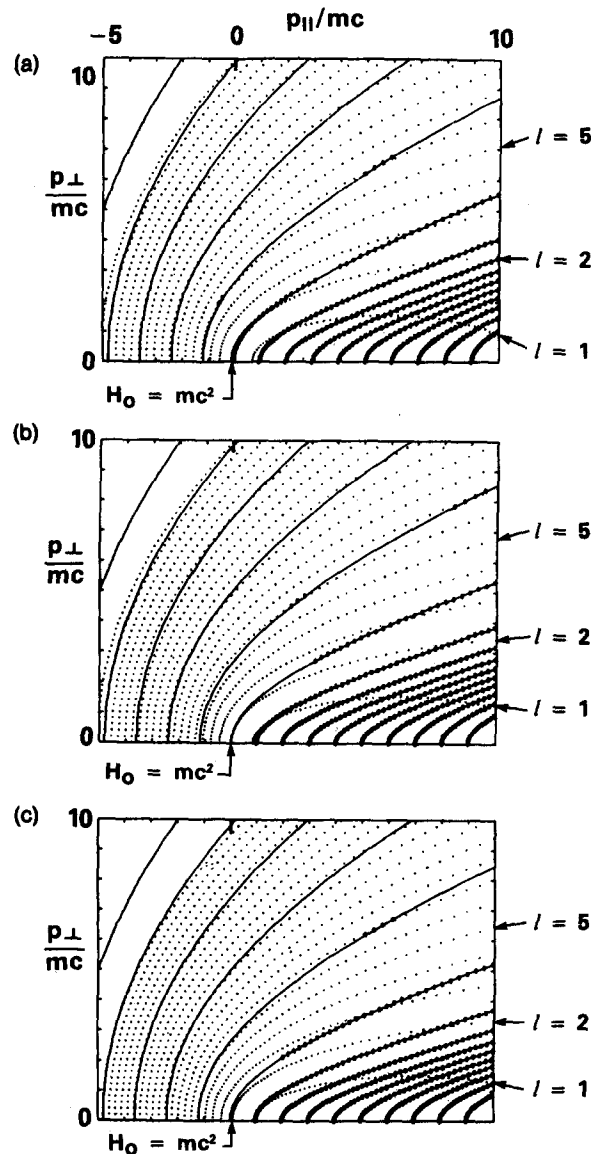


FIG. 3. Resonance diagrams ( $\omega_p/\omega_c = 0.3$ ,  $\alpha = 10^\circ$ ,  $\epsilon = 0.3$ ). (a)  $\omega/\omega_c = 1.8$ , (b)  $\omega/\omega_c = 2.0$ , (c)  $\omega/\omega_c = 2.2$ .

except when  $\omega/\omega_c = 1.8$ . As we shall discuss in more detail when comparing the resonance diagrams to surface-of-section plots, KAM surfaces appear that block electron acceleration when  $\omega/\omega_c = 2.0$  or  $2.2$  for the parameters of Fig. 3. For this reason, most of our examples consider frequencies just below multiples of the cyclotron harmonic, particularly at small angles where this effect is more pronounced. In Fig. 4, we show resonance diagrams for the frequency range  $\omega/\omega_c = 2.8$ – $4.8$ . Figures 3(a) and 4 indicate that in the frequency range 1.8–4.8 there is a slow falloff in the resonance widths as the frequency increases.

Similar behavior is visible at all angles and amplitudes we examined. There is a slow falloff in the resonance widths as  $\omega/\omega_c$  increases, and one finds that beyond some point it is no longer possible to accelerate electrons from zero kinetic energy. More important than this weak falloff is the increased power flux required to attain a given value of  $\epsilon$ . The relationship is

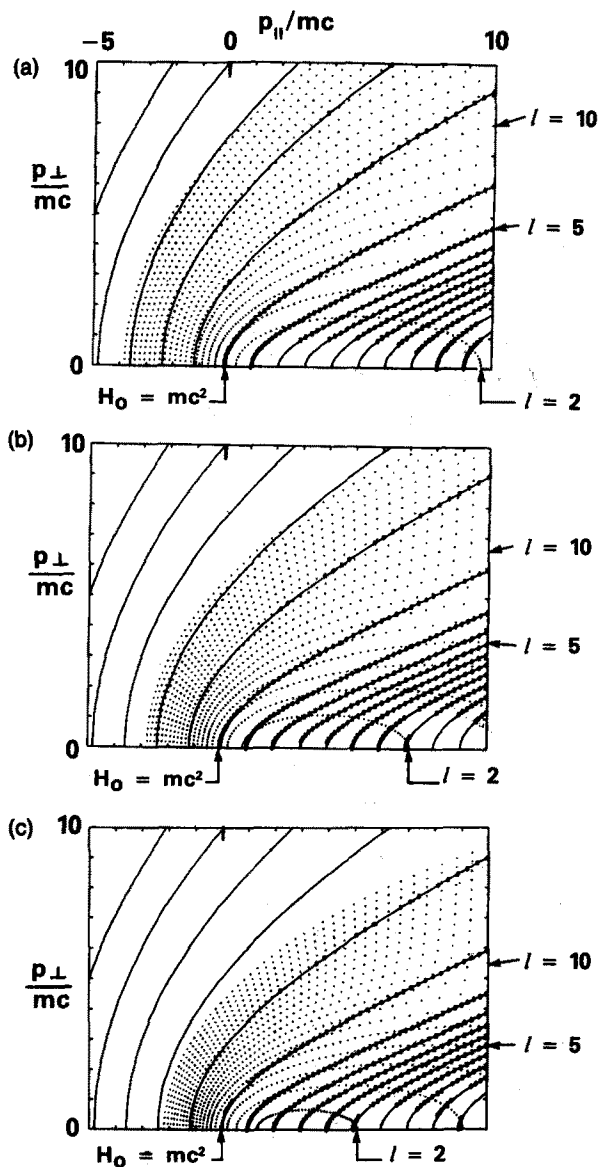


FIG. 4. Resonance diagrams ( $\omega_p/\omega_c = 0.3$ ,  $\alpha = 20^\circ$ ,  $\epsilon = 0.2$ ). (a)  $\omega/\omega_c = 2.8$ , (b)  $\omega/\omega_c = 3.8$ , (c)  $\omega/\omega_c = 4.8$ .

$$P \approx 30 \left( \epsilon \frac{\omega}{\omega_c} \right)^2 \text{ W/cm}^2. \quad (35)$$

Thus there is a quadratic increase in the power flux required as  $\omega$  increases. We conclude that the power requirement is lowest at the smallest frequencies possible before propagation effects become important.

We now consider the effect of setting  $\omega_p/\omega_c = 2$ , corresponding to the weakly magnetized limit or the daytime ionosphere at a height between 110 and 120 km. In this case, the frequency  $\omega/\omega_c$  is bounded by the condition  $\omega_p^2/[\omega(\omega - \omega_c)] < 1$  to values  $\omega/\omega_c > 2.6$ . In Fig. 5 we show resonance diagrams for  $\omega/\omega_c = 3.0$ , and in Fig. 6 we show resonance diagrams for  $\omega/\omega_c = 4.0$ . These diagrams indicate that when  $\omega/\omega_c = 3.0$ , no significant electron acceleration occurs, while when  $\omega/\omega_c \geq 4.0$ , it is possible to accelerate electrons to 5 MeV and more if  $\alpha > 60^\circ$  and  $\epsilon = 0.3$ . A complete examination of resonance diagrams in the range  $3.0 < \omega/\omega_c < 4.0$  indicates that  $\omega/\omega_c > 3.8$  is the

condition for significant acceleration. Comparing Figs. 5 and 6, one sees that the resonances grow more closely spaced as  $\omega/\omega_c$  increases, which appears to account for the difference.

A complete examination of resonance diagrams shows that when  $\alpha < 60^\circ$ , no significant acceleration occurs at any frequency. As  $\omega/\omega_c$  increases beyond 4.0, there is a slow falloff of the resonance widths, similar to that observed in the strongly magnetized case.

## B. Surface-of-section plots

The resonance diagrams, based on Chirikov's approach,<sup>11</sup> are calculated perturbatively. We now turn to the study of single particle orbits, using surface-of-section plots, to determine the reliability of the resonance diagrams. We have found that the resonance diagrams yield reliable results in all the cases we examined, indicating to within a factor of 2 the amplitudes at which substantial acceleration occurs. The method for generating surface-of-section plots from the particle trajectories obtained by solving the equations of motion has been well described elsewhere.<sup>11,12</sup> In brief, the Hamiltonian  $H(p_z, z, J, \theta)$  is a constant of the motion; hence all trajectories with the same Hamiltonian value reside on a three-dimensional surface in phase space. If for each trajectory we now plot either the point  $(z, p_{\parallel})$  or the point  $(p_{\parallel}, p_{\perp})$  whenever  $\theta$  returns to zero, we find that two possibilities exist. The trajectory is regular, in which case the points are located along a one-dimensional curve, or the trajectory is stochastic, in which case the points fill a two-dimensional region densely. For the purpose of acceleration, the stochas-

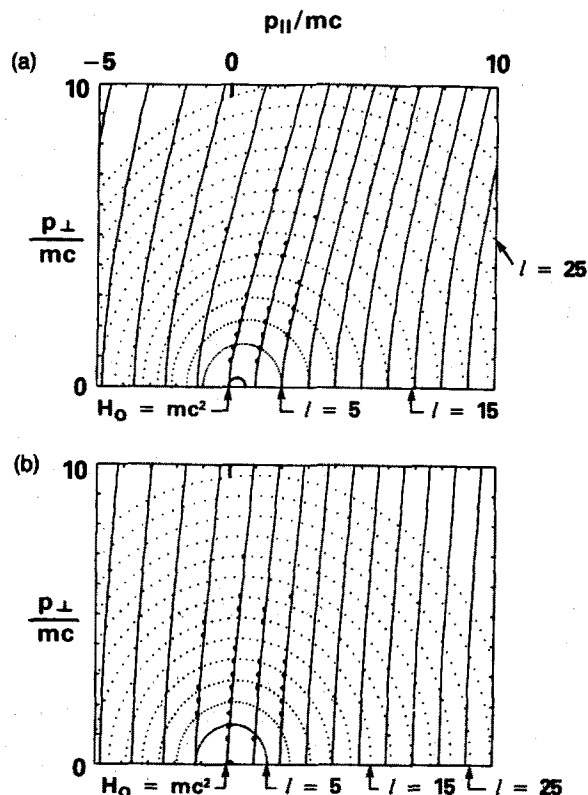


FIG. 5. Resonance diagrams ( $\omega/\omega_c = 3.0$ ,  $\omega_p/\omega_c = 2.0$ ,  $\epsilon = 0.3$ ). (a)  $\alpha = 60^\circ$ , (b)  $\alpha = 80^\circ$ .

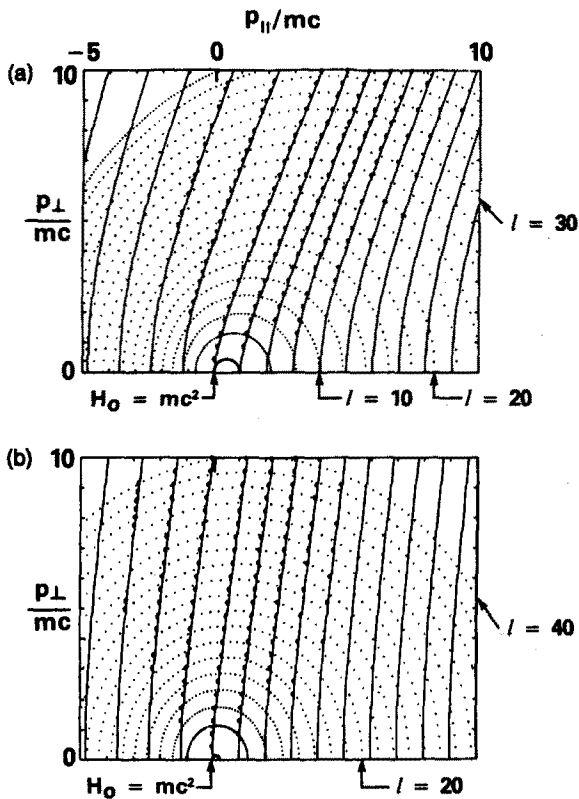


FIG. 6. Resonance diagrams ( $\omega/\omega_c = 4.0$ ,  $\omega_p/\omega_c = 2.0$ ,  $\epsilon = 0.3$ ). (a)  $\alpha = 60^\circ$ , (b)  $\alpha = 80^\circ$ .

tic trajectories are good since electrons on them can achieve high energies, while regular trajectories are bad. Not only do electrons on these trajectories not accelerate, but these trajectories can act as KAM barriers to the continued acceleration of stochastic electrons.<sup>6,11,12</sup>

We have made comparisons of resonance diagrams and surface-of-section plots in 30 cases covering the parameter ranges of interest with  $H_0 = mc^2$  in all cases. In Fig. 7 we exhibit a typical comparison. We use a variable time step, variable order, Adams-Bashforth approach to solve for the particle orbits in the surface-of-section plots.

In Fig. 8 we show surface-of-section plots corresponding to the  $H_0 = mc^2$  surface in Fig. 3. When  $\omega/\omega_c = 1.8$ , the  $l = 2$  resonance occurs at a sufficiently high  $p_{\parallel}$  value so that the acceleration of electrons from zero kinetic energy is not obstructed, although it is impeded somewhat because of stickiness. By contrast, when  $\omega/\omega_c = 2.0$  or  $2.2$ , KAM surfaces appear near  $p_{\parallel} = 0$ , blocking acceleration from zero kinetic energy.

#### IV. THE rf ACCELERATION OF IONOSPHERIC ELECTRONS

We now apply our results to determine the power density that would have to be achieved by ground based rf facilities to create large fluxes of relativistic electrons in the ionosphere. Such a technique, if it proves successful, will have important consequences in the area of ionospheric and magnetospheric modifications and probing. The model of the ionosphere and wave propagation that we are considering is

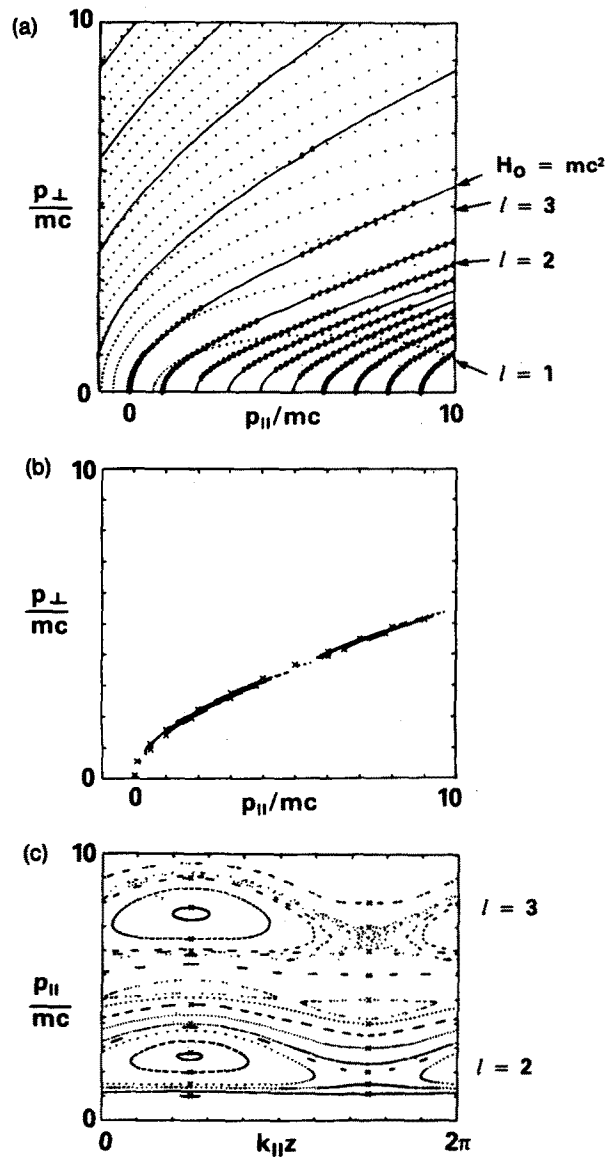


FIG. 7. Comparison of resonance diagrams and surface-of-section plots ( $\omega/\omega_c = 1.8$ ,  $\omega_p/\omega_c = 0.3$ ,  $\alpha = 10^\circ$ ,  $\epsilon = 0.1$ ). (a) Resonance diagram, (b)  $p_{\parallel}$ - $p_{\perp}$  surface-of-section plots, (c)  $k_{\parallel}$ - $z$ - $p_{\parallel}$  surface-of-section plot. On the surface of section, an  $\times$  indicates the initial condition. Twenty trajectories were followed.

idealized in a number of important respects: We have used standard, averaged values for the daytime and nighttime ionospheres, neglecting the effects of spatial and temporal inhomogeneities. We also have not examined self-consistent effects or the effect of finite bandwidth, although these are not expected to be of great importance. Finally, and most important, we do not consider propagation and accessibility issues; these must be addressed before we can determine whether the necessary power can be focused into the interaction region. Nonetheless, our approach does provide a useful estimate of the wave power parameters needed to achieve significant acceleration in a given region of the ionosphere.

We stress also that the stochastic acceleration mechanism described here, because of its robustness, is certain to play an important role in a wide variety of space and astro-



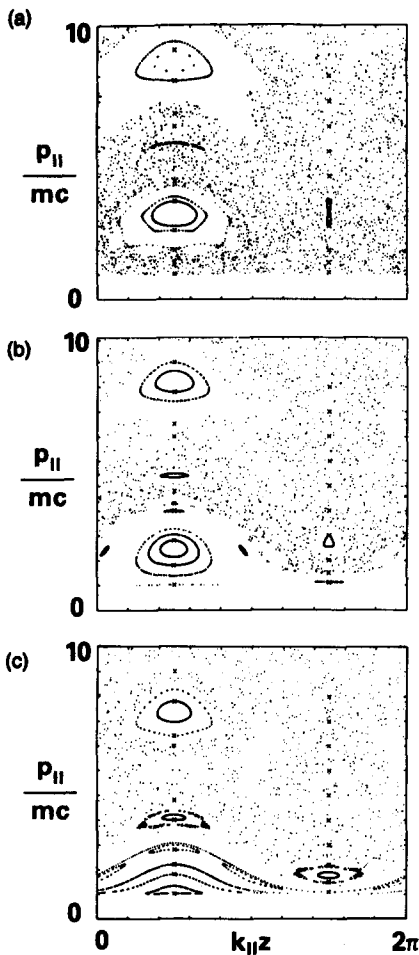


FIG. 8. Surface-of-section plots for the same parameters as in Fig. 3.

physical settings. An example is the Crab Nebula,<sup>15</sup> which will be discussed in detail elsewhere.

Using simple scaling arguments,<sup>6</sup> we find that during one trapping time in the wave  $\tau = 1/\omega\epsilon^{1/2}$ , the change in momentum is roughly  $mce^{1/2}$ . Assuming that the electron motion is chaotic, we find

$$\langle (\Delta p)^2 \rangle^{1/2} \sim (mce^{1/2})(t/\tau)^{1/2} = mce^{3/4}(\omega t)^{1/2}, \quad (36)$$

where  $\langle (\Delta p)^2 \rangle^{1/2}$  is the average momentum change of the electron distribution. Equation (36) is expected to underestimate significantly the time needed to achieve a given  $\langle (\Delta p)^2 \rangle^{1/2}$  since it does not take into account the Bessel function factors or stickiness. Since it minimizes the power consumption to operate as close as possible to the stochasticity threshold, stickiness can play an important role. Simulations to be presented shortly support this conclusion. As we shall verify shortly, the parallel electron velocity is approximately  $c \cos \alpha$  during most of the acceleration process when  $\epsilon$  is well above the stochasticity threshold. Hence we find

$$\langle (\Delta p)^2 \rangle^{1/2} \sim mce^{3/4}[\omega z/(c \cos \alpha)]^{1/2} \quad (37)$$

as the electrons pass through the acceleration region.

Equation (37) indicates that large angles are preferable for accelerating electrons when attempting to maximize the fraction of electrons that achieves a given energy over a fixed distance. However, there is a counterbalancing geometric

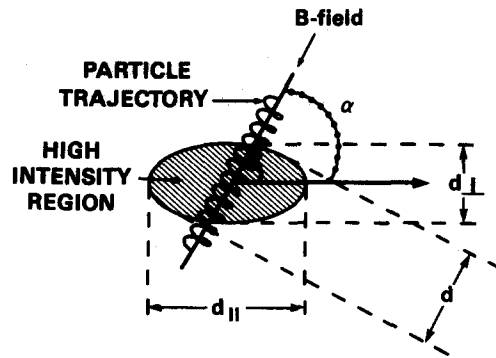


FIG. 9. Schematic illustration of the acceleration region geometry.

effect that must be taken into account; the high intensity region where electrons are accelerated will be longer along the direction of propagation than perpendicular to it, as shown in Fig. 9. The ratio  $r$  of parallel to perpendicular length depends on the details of the transmission system. The length  $d$  that electrons travel along the propagating region is given by

$$d = d_{||} / (\cos^2 \alpha + r^2 \sin^2 \alpha)^{1/2}, \quad (38)$$

where  $d_{||}$  is the length of the interaction region in the direction of propagation. Thus the time spent in the interaction region is

$$t = d / (c \cos \alpha) = (d_{||}/c) / (\cos^2 \alpha + r^2 \sin^2 \alpha)^{1/2} \cos \alpha. \quad (39)$$

We find that if  $r < 2$ , the interaction time is a *minimum* along the direction of propagation. If  $2 < r < \infty$ , the minimum is somewhere between  $\alpha = 0^\circ$  and  $\alpha = 45^\circ$ . In Fig. 10 we show the residence time as a function of  $\alpha$  when  $r = 4$ . In all cases the residence time is maximized by using large angles.

To justify our previous statement that  $v_z \approx c \cos \alpha$ , we use Eq. (19) to obtain

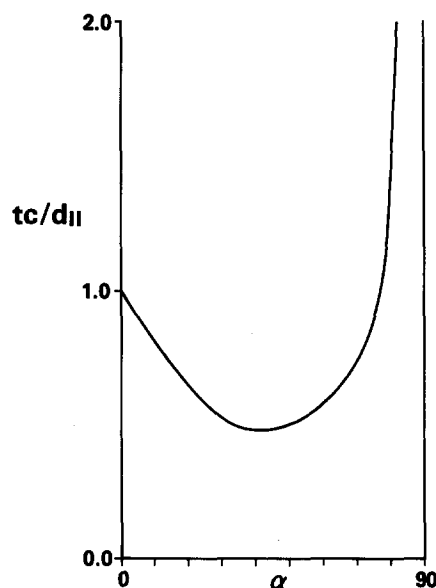


FIG. 10. Plot of residence time versus angle of propagation.

$$1 = \gamma - (\gamma v_z/c)/(n \cos \alpha), \quad (40)$$

on the  $H_0 = mc^2$  surface, where we have dropped the 0 subscript in Eq. (19) and employed the relation  $p_z = \gamma m v_z$ . We conclude

$$v_z = [(\gamma - 1)n/\gamma]c \cos \alpha. \quad (41)$$

When  $n \approx 1$ ,  $v_z \rightarrow c \cos \alpha$  as  $\gamma$  increases.

We now turn to the results of our simulations. We consider the following set of parameters:  $\omega_p/\omega_c = 0.3$ ,  $\omega/\omega_c = 2.0$ ,  $\epsilon = 0.2$ , and  $\alpha = 80^\circ$ . At this value of  $\epsilon$  the stochasticity threshold is well exceeded. These parameters correspond to the nighttime ionosphere at roughly 130 km, a power flux of 20 W/cm<sup>2</sup>, and a frequency of 2.6 MHz. In Fig. 11 we exhibit histograms of the electron number versus the relativistic factor at various times. There are 256 electrons and they start at  $\gamma = 1$ , spread evenly over the different initial values of  $\psi = k_{\parallel}z + k_{\perp}x$ . The equations of motion are integrated using a variable order, variable time step Adams–Bashforth approach, just as in the surface-of-section plots. The diffusive nature of the energy increase is evident. In Fig. 12 we show a similar set of histograms of the electron distance. While they are peaked at the maximum distance,  $d = ct \cos \alpha$ , there is a considerable spread. In Table I we show the fraction of electrons that reaches a value of  $\gamma = 10$ , corresponding to roughly 5 MeV.

In Figs. 13 and 14 we show similar results for almost the same parameter set as in Figs. 11 and 12:  $\omega_p/\omega_c = 0.3$ ,  $\omega/\omega_c = 2.0$ , and  $\alpha = 80^\circ$ . The only difference is that  $\epsilon$  is equal to 0.1 rather than 0.2. These parameters correspond to Fig. 2(c). At this value of  $\epsilon$ , the field amplitude is only slightly

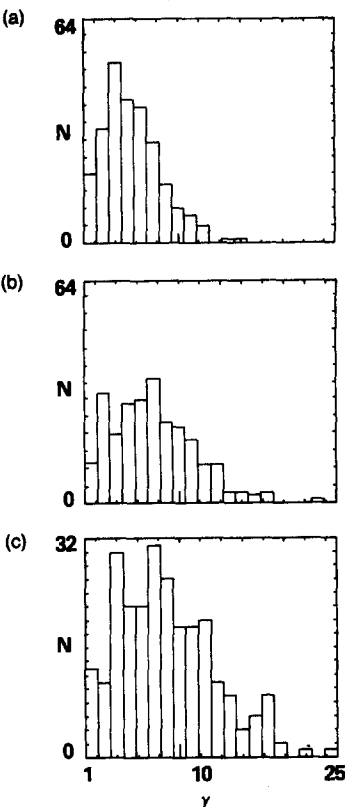


FIG. 11. Histogram of particle number versus  $\gamma$  ( $\epsilon = 0.2$ ). (a)  $\omega_c t = 1000$ , (b)  $\omega_c t = 2000$ , (c)  $\omega_c t = 3000$ .

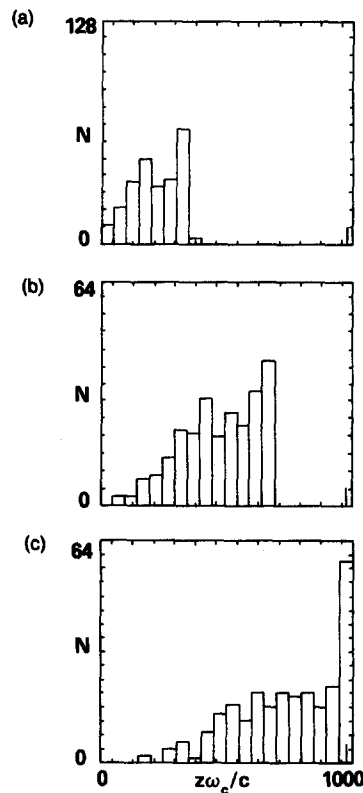


FIG. 12. Histogram of particle number versus parallel distance ( $\epsilon = 0.2$ ). (a)  $\omega_c t = 1000$ , (b)  $\omega_c t = 2000$ , (c)  $\omega_c t = 3000$ .

above the stochasticity threshold, and the effect of stickiness is apparent. While a substantial fraction of electrons is able to accelerate to high energies, a substantial fraction is also confined below 1 MeV. Because of the stickiness, Eqs. (36) and (37) are not useful guides to the electron behavior in this case.

We now consider the possibility of accelerating electrons in a region of the ionosphere 20 km  $\times$  10 km. In this case, the area covered is  $2 \times 10^{12}$  cm<sup>2</sup>. The total power required when  $\epsilon = 0.1$  is thus  $10^{13}$  W. If we launch 1 msec pulses with a duty cycle of 1 per minute, we find an average power of  $10^8$  W. These values may be realizable using modern-day technology and open up the exciting possibility of using remotely excited electrons as near-space probes.

## V. CONCLUSIONS

We have considered electron acceleration in the field of intense electromagnetic waves. We found that above a certain critical intensity threshold electron motion becomes stochastic. In addition, when the parallel phase velocity is supraluminous, the Hamiltonian surfaces are topologically

TABLE I. Fraction of electrons with  $\gamma > 10$  and the average distance traveled when  $\omega_p/\omega_c = 0.3$ ,  $\omega/\omega_c = 2.0$ ,  $\alpha = 80^\circ$ , and  $\epsilon = 0.2$ .

$F(\gamma > 10)$	$\omega_c t$	$\bar{z}(\epsilon = 0.2)$
0.005	500	3 km
0.08	1000	7 km
0.25	2000	18 km
0.36	3000	27 km

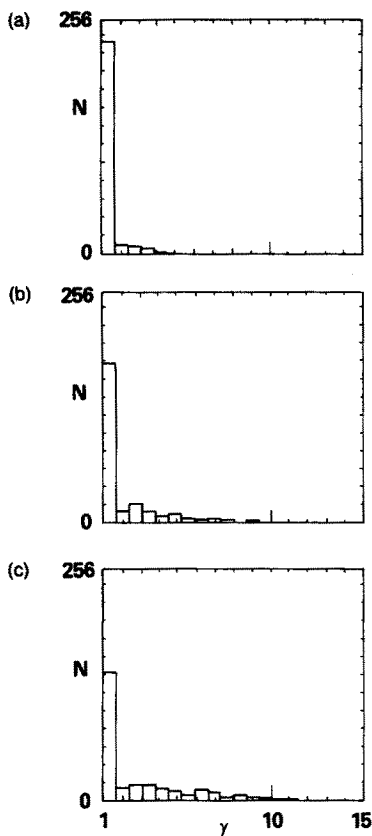


FIG. 13. Histogram of particle number versus  $\gamma$  ( $\epsilon = 0.1$ ). (a)  $\omega_c t = 1000$ , (b)  $\omega_c t = 2000$ , (c)  $\omega_c t = 3000$ .

open and the electrons can gain truly enormous amounts of energy. While electron energy gains can be substantial below the stochasticity threshold, they are limited by the trapping width of a single resonance. Above the stochasticity threshold no such limitation applies. In addition, the stochastic mechanism is robust. It is only weakly sensitive to shifts in the wave's frequency and angle of propagation, in sharp contrast to coherent acceleration mechanisms. As a consequence, the stochastic mechanism is ideally suited to space applications and is certain to have applications in a wide array of space and astrophysical settings.

To determine the intensity threshold condition and the attainable energies, we used resonance diagrams based on the overlap criterion. These diagrams are rapidly calculable, allowing us to explore a broad range of parameters. The accuracy of these diagrams was verified using surface-of-section plots. The results of this study were then applied to determine the conditions under which substantial fluxes of high energy ionospheric electrons could be obtained using ground-based rf transmitters. Using simple simulations, we found that it may be possible to achieve the desired acceleration using present-day technology, opening the door to a variety of interesting applications.

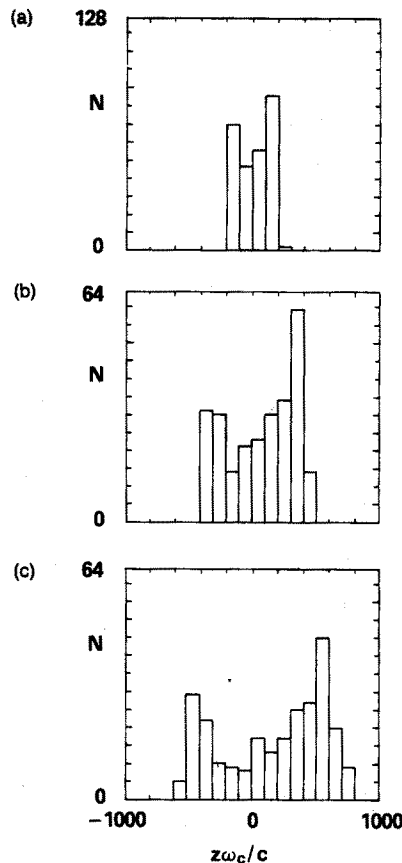


FIG. 14. Histogram of particle number versus parallel distance ( $\epsilon = 0.1$ ). (a)  $\omega_c t = 1000$ , (b)  $\omega_c t = 2000$ , (c)  $\omega_c t = 3000$ .

- <sup>1</sup>A. A. Kolomenskii and A. N. Lebedev, *Sov. Phys. Dokl.* **7**, 745 (1963); *Sov. Phys. JETP* **17**, 199 (1963).
- <sup>2</sup>C. S. Roberts and S. J. Buchsbaum, *Phys. Rev.* **135**, A381 (1964).
- <sup>3</sup>P. Sprangle and L. Vlahos, *Astrophys. J. Lett.* **337**, L95 (1983).
- <sup>4</sup>J. P. Ostriker and J. G. Gunn, *Astrophys. J.* **157**, 1395 (1969).
- <sup>5</sup>See, e.g., *Laser Acceleration of Particles*, AIP Conference Proceedings No. 98, edited by P. J. Channel (American Institute of Physics, New York, 1982) and *Advanced Accelerator Concepts*, AIP Conference Proceedings No. 156, edited by F. E. Mills (American Institute of Physics, New York, 1986) for reviews of laboratory applications.
- <sup>6</sup>C. R. Menyuk, A. T. Drobot, K. Papadopoulos, and H. Karimabadi, *Phys. Rev. Lett.* **58**, 2071 (1987).
- <sup>7</sup>T. Tajima and J. M. Dawson, *Phys. Rev. Lett.* **43**, 267 (1979).
- <sup>8</sup>T. Katsouleas and J. M. Dawson, *Phys. Rev. Lett.* **51**, 392 (1983).
- <sup>9</sup>G. R. Smith and A. N. Kaufman, *Phys. Fluids* **21**, 2230 (1978).
- <sup>10</sup>C. R. Menyuk, *Phys. Fluids* **26**, 705 (1983).
- <sup>11</sup>B. V. Chirikov, *Phys. Rep.* **52**, 263 (1979).
- <sup>12</sup>A. J. Lichtenberg and M. A. Lieberman, *Regular and Stochastic Motion* (Springer, New York, 1983), pp. 17–20.
- <sup>13</sup>J. R. Winckler, *Rev. Geophys. Space Phys.* **18**, 659 (1980).
- <sup>14</sup>K. Papadopoulos, in *Artificial Particle Beams in Space Plasma Studies*, edited by B. Grandal (Plenum, New York, 1982), p. 409.
- <sup>15</sup>H. Karimabadi, Ph.D. thesis, University of Maryland, 1988.
- <sup>16</sup>This generating function is what Goldstein defines as an  $F_2(p, q)$ . See H. Goldstein, *Classical Mechanics* (Addison-Wesley, Reading, MA, 1981), pp. 378–385.
- <sup>17</sup>Y. L. Alpert and D. S. Fligel, *Propagation of ELF and VLF Waves Near the Earth* (Consultants Bureau, New York, 1970), p. 7.
- <sup>18</sup>A. V. Gurevich, *Nonlinear Phenomena in the Ionosphere* (Springer, New York, 1978), pp. 2, 3, 100, and 101.